Dynamics of Laboratory Diapir and Plume Models

JOHN A. WHITEHEAD, JR.

Department of Physical Oceanography, Woods Hole Oceanographic Institution
Woods Hole, Massachusetts 02543

DOUGLAS S. LUTHER

Woods Hole Oceanographic Institution, Woods Hole, Massachusetts 02543
Massachusetts Institute of Technology, Cambridge, Massachusetts 02139

The low Reynolds number dynamics of a thin layer of fluid bounded below by a flat horizontal boundary and moving buoyantly through a fluid of another viscosity and density is observed by means of model experiments and is described theoretically. Three distinct stages of growth were observed. The first stage is described by a linearized Rayleigh-Taylor instability, for which previous literature, present theory, and experiments exhibit close agreement. In this stage, disturbances of one specific wave number are found to grow most rapidly. In the second stage, distortion of the interface is large enough to invalidate the linearized analysis. It is found experimentally that the fluid moves upward as circular columns surrounded by relatively broad regions of descending material. A theory is advanced that attributes an accelerated growth to a structure of this kind through a resonant triad interaction. In the third stage, fully matured structures are formed. If the upwelling material has greater viscosity than the surrounding material, the structure is a long vertical column with gradually decreasing diameter; if the upwelling material has less viscosity than the surrounding material, the structure develops a rim syncline and a pronounced overhang and eventually ascends as a spherical pocket of fluid fed by a pipe. Dynamic explanations for these features are advanced, and some possible implications for geological and geophysical processes are discussed.

A number of theories about the internal horizontal structure of the mantle involve hot spots, mantle plumes, pipes, ascending sheets of fluid under ridges, ascending blobs of fluid under island arc chains, and the like. More needs to be done to reconcile the possibility of such structures with what is known of flow in a deformable material.

Likewise, on a smaller scale, various types of diapirs are believed to be formed from a density inversion. Perhaps the most highly studied example is salt domes, a considerable amount being known about the structure of the domes and the fluid properties of salt at elevated temperature. However, a variety of other diapiric structures possibly have similar dynamic origins, such as granitic batholiths, mud volcanoes, mud lumps, and clay diapirs. Survey papers and a recent bibliography are given by *Braunstein and O'Brien* [1968].

As an attempt to understand such structures, this paper is concerned with the qualitative shape and quantitative dynamics that occur when a fluid of a given large viscosity moves buoyantly up or down through a fluid of another large viscosity and density in a field of gravity. We report on experiments in which a thin horizontal layer of fluid is observed to go unstable and deform to a matrix of upwelling spouts that rise through a denser fluid of another viscosity. It is observed that the structural features are strongly dependent on which fluid is more viscous. The dynamics of such a process is discussed. Experiments in which a fluid is fed from a continuous source are described, and it is again noted that the structural features are strongly dependent on which fluid is more viscous. Theories for the formation of the structures are advanced by using Newtonian fluid dynamics. Lastly, a comparison with some diapiric formations will be made.

Of the theoretical and laboratory studies of diastrophic movements that have been previously modeled by theory or in laboratories, the greatest number were aimed specifically at the salt dome problem.

The investigations have utilized essentially two approaches. In the first the materials have been assumed to be Newtonian fluids. Analytical results were then obtained for the growth rates of disturbances in a fluid that is initially almost perfectly flat. This problem has been formulated by, among others, *Daneš* [1964], solved theoretically by *Selig* [1965], solved also by *Biot and Odé* [1965] and *Biot* [1966], and solved numerically for many layers by *Ramberg* [1968*a*, *b*]. In all cases the equations could be solved analytically as a linearized problem, and recourse to a computer was necessary only to avoid heavy algebraic manipulation. Recently, *Berner et al.* [1972] have used finite difference methods to study more matured structures that cannot be studied analytically. Emphasis in all the papers was confined to the range of parameters believed to be important in salt domes.

Experimental observations of such a Newtonian fluid were made by *Nettleton* [1934] and *Dobrin* [1941] in which clear photographs and detailed qualitative discussion revealed that such domes possess many features of real salt domes, although no theories were advanced to explain the features of the structures.

The second approach has been to study the instability of materials whose rheology is felt to be somewhat more earthlike. Because of uncertainty in the rheological equations, very little theoretical or quantitative work is possible, and the articles are confined to describing qualitative features of the intrusions. An extensive work of this nature is by *Parker and McDowell* [1955], which also contains an excellent bibliography of earlier work. A second set of qualitative experimental studies has been done by *Ramberg* [1963, 1967, 1970], who subjected specimens of pasty material to centrifugal forces. This approach has the distinct advantage that relatively complex and realistic geometries are easily studied,

and specimens can be stored and studied for a relatively long period of time.

The present paper differs from these earlier works in that a large range of viscosities is studied theoretically, and experiments are conducted for the limiting cases.

OBSERVATIONS OF UNSTABLE LAYERS

This section will describe some simple experiments that were performed in order to visualize the problem. The experiments were suggested by D. Griggs after a seminar given by D. Chappell at the Institute of Geophysics and Planetary Physics, University of California at Los Angeles, in 1969. A container was almost completely filled with glycerin with a kinematic viscosity of 1400 cm^2/s and a density of 1.25 g/cm^3, to which a small amount of immiscible silicone oil with a viscosity of 60,000 cm^2/s and a density of 0.92 g/cm^3 was added. This formed a layer on top of the glycerin approximately 5 mm thick. The container was then carefully covered so that no air was left in it. After being left overnight, the container was inverted. In about 30 s the layer of viscous oil (which was on the bottom of the tank) was observed to develop protrusions that buoyantly pushed upward through the glycerin as long buoyancy-driven columns, shown in the series of photographs in Figure 1. We found in particular, that if the container was left carefully leveled for a number of days so that the oil interface was very flat before inversion, the columns that developed were spaced quite uniformly throughout the tank and were very nearly equal in size, volume, and growth rate. The wave number of the columns, defined as $2\pi H/L$, where L is the distance between columns and H is the depth of the fluid, was 2.5.

The same experiment was performed with another container filled almost completely with silicone oil and with a thin layer of glycerin on the bottom. Again, after the container was carefully leveled and left for a couple of days, a series of protrusions developed shortly after inversion. These protrusions also arranged themselves quite uniformly throughout the tank, but the wave number in this case was much less, 0.63. The finite amplitude behavior of these protrusions was dramatically different from that of the previous case. The protrusions formed fat spherical pockets of fluid that gradually developed pronounced overhang to the point where the neck of fluid feeding these pockets almost pinched off and left a tiny pipe of fluid trailing the main pocket of fluid, which descended through the viscous fluid as almost perfect spheres. This sequence is shown in Figure 2. The pictures are inverted for clarity.

It appears that the unstable flows proceeded through three distinct physical flow stages, which will be discussed in the next three sections. Initially, the surface was nearly flat, while small distortions to the interface grew by a Rayleigh-Taylor instability. During this stage the assumption of an almost flat surface allows the equations to be linearized, and the equations that describe the growing flow have long been known. Such a study predicts the wavelength of maximum growth and the exponential time constant of growth. The predicted rates, which will be described in the next section, agree with various observations in the literature as well as with observations in the experiment described here.

The second stage occurred when the interface became distorted enough to violate the linearizing assumptions of the first stage. More complicated physical processes that generally have not been identified began to occur at this stage. A few of the things that can happen are enhanced growth rate (superexponential), nonlinear interactions among the various growing modes, and a consequential narrowing of the class of the fastest growing modes. A work discussing this stage will be briefly described in the section on the initiation of spouts.

In the third stage the interface was greatly distorted, and the intrusions had developed a matured structure. The linearized solutions now are completely inadequate for describing the flow. The experiments indicated that this final state is also a strong function of the ratios of the viscosities of the two fluids. The dynamics of these structures will be hypothesized and tested against experiment. These will be described in the section on rim synclines, overhang, and 'necking.'

INITIAL INSTABILITY

The Rayleigh-Taylor instability has been described elsewhere and will be only briefly reviewed here. The algebra used to derive these relations is in Appendix 1. The coordinate notation is shown in Figure 3.

When the interface between a thin layer of fluid and an overlying region of denser fluid is slightly distorted, a small

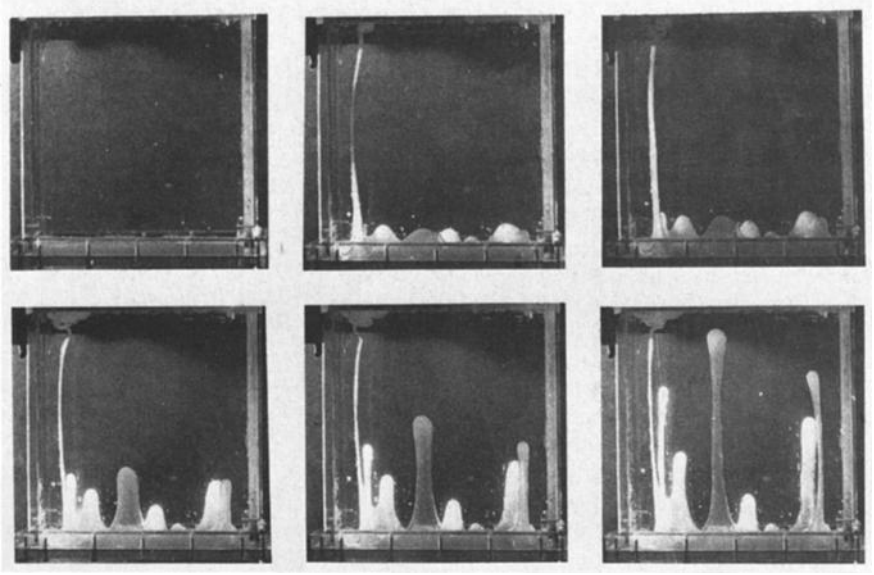

Fig. 1. A thin layer of viscous fluid protruding into a fluid with 1/44 its viscosity.

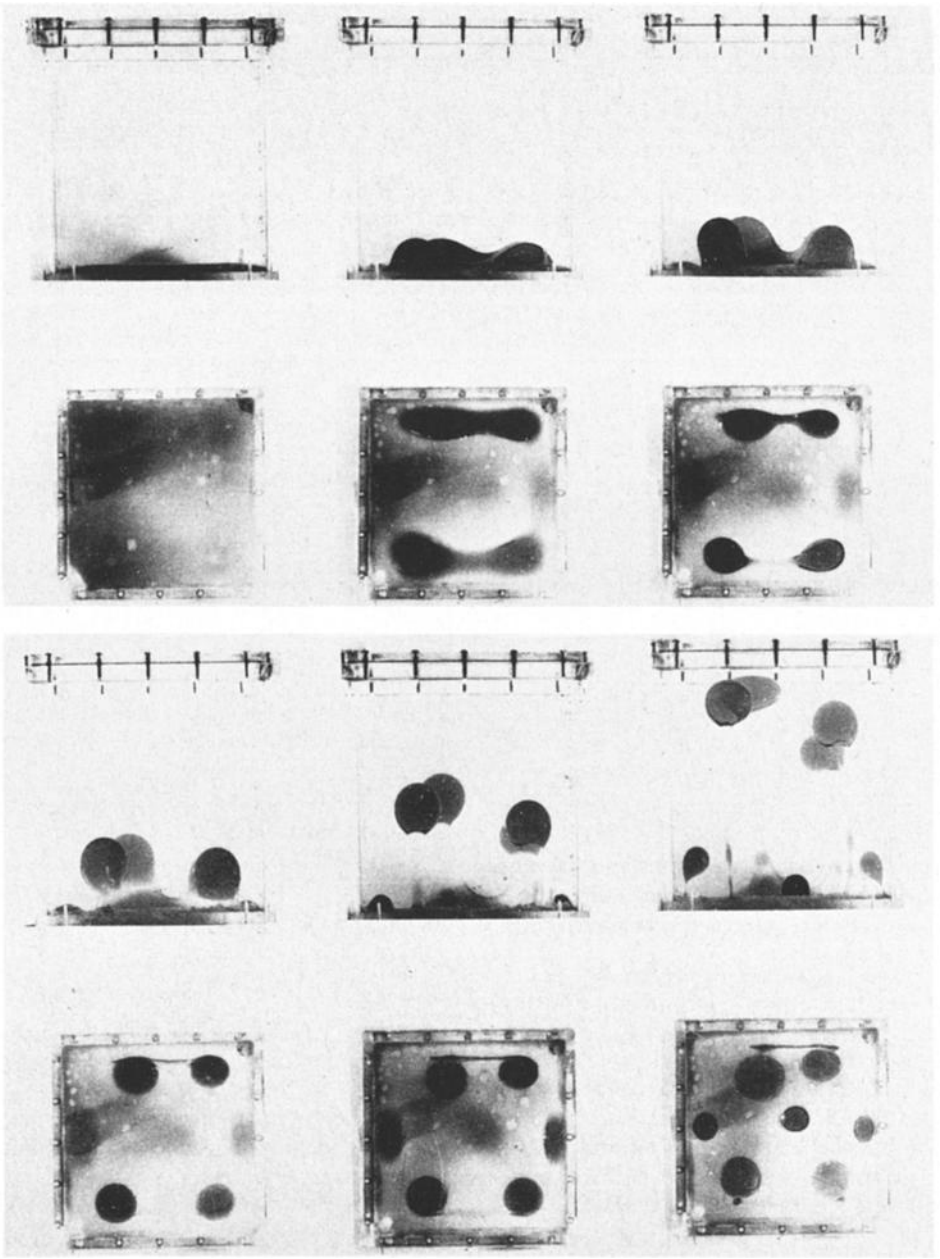

Fig. 2. A thin layer of fluid protruding into a fluid with 44 times its viscosity.

pressure gradient is created in the horizontal direction. In a viscous fluid a slow flow will thus be created, no matter how small the pressure; the same is not true of a plastic material. To a first approximation, distortion of the interface arises from vertical movements; i.e., $\partial\eta/\partial t = w(z = 0)$. when η is the interface that was originally at $z = 0$. This flow can be fully described theoretically, as is demonstrated in Appendix 1, and the solution to both regions is of the form

$$W = f(z)\, g(x, y)e^{nt} \tag{1}$$

where W is the velocity in the z (vertical) direction and $f(z)$ is the solution to the equation

$$(D^2 - k^2)^2 f(z) = 0 \tag{2}$$

where D is a derivative with respect to z. The function $g(x, y)$ satisfies the equation

$$(\partial^2/\partial x^2 + \partial^2/\partial y^2)\, g(x, y) = -k^2 g(x, y) \tag{3}$$

The class of periodic functions that satisfy such an equation is infinite, but some simple functions are sin ($\mathbf{k}\cdot\mathbf{x}$) or cos ($\mathbf{k}\cdot\mathbf{x}$) (where $\mathbf{k}$ is a vector in some arbitrary horizontal direction), Bessel functions, and the sums or differences of such functions. Because of the generality of (3), the linearized Rayleigh-Taylor analysis is not very specific about the x-y dependence of the flow but can only indicate that the flow is described by some horizontal length scale $2\pi/k$. We must wait for more processes to act from the nonlinear aspects of finite distortion of the surface before we can be more specific about horizontal structure. For given boundary conditions on $f(z)$ the growth rate n is a function only of the magnitude of wave number k, and obtaining this dependence involves solving for the matching conditions at the interface. Results have been derived by *Selig* [1965] for a single layer penetrating into an infinite fluid and by *Ramberg* [1968*a*] for many layers. When the viscosity of the thin layer is very large, growth rate as a function of wave number is derived in Appendix 1 and is sketched in Figure 4. The wave number of fastest growth is

$$k_m = (180\epsilon)^{1/5}/2h \tag{4}$$

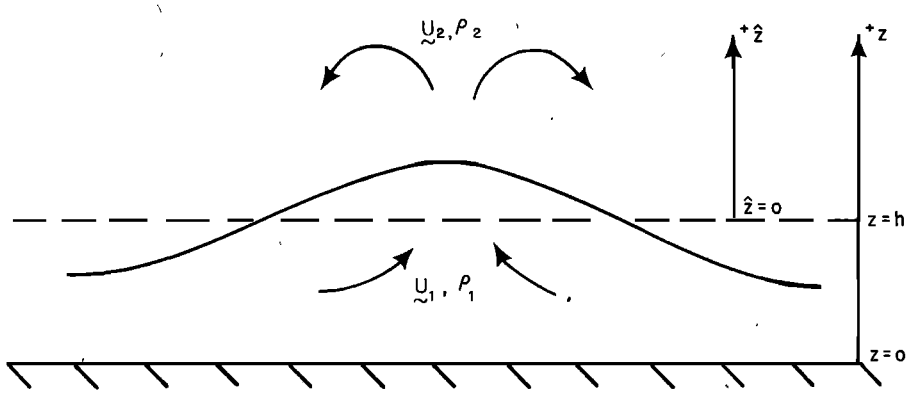

Fig. 3. Sketch of the system studied and definition of coordinates.

where h is the depth of the thin layer, $\epsilon = \mu_2/\mu_1$ (μ_1 being the viscosity of the thin layer and μ_2 being the viscosity of the infinitely deep layer), and the growth rate is

$$n = (-g\Delta\rho h/4\mu_1)(1 - 0.443\epsilon^{4/5}) \tag{5}$$

Note that the growth rate is determined almost entirely by the large-viscosity fluid. The results for very large ϵ are sketched in Figure 5 for a free slip boundary below the thin layer,

$$k_m = 2.88\epsilon^{-1/3}/2h \qquad n = 0.232\ (g\Delta\rho h/\mu_2)\epsilon^{-1/3} \tag{6}$$

and for Selig's case with no slip (his equations (2.11)),

$$k_m = 2.15\epsilon^{-1/3}/h \qquad n = 0.153\ (g\Delta\rho h/\mu_2)\epsilon^{-1/3} \tag{7}$$

The boundary conditions affect the constants in these equations slightly but do not affect the power laws, as can be seen by examining the equations governing n as a function of k or by using variational arguments.

Initiation of Spouts: The Effect of Finite Amplitude

In the last section it was emphasized that the horizontal structure of the solutions to the linear stability problem is not unique. As distortion of the interface becomes large, the effects of the distortion can narrow the range of the fastest growing solutions, and a theory of the means by which this is done is given in Appendix 2. The basic idea is similar to earlier ideas about the behavior of Bénard cells, which can arise in fluid heated from below having temperature-dependent physical properties [*Busse*, 1962] or time-dependent behavior [*Krishnamurti*, 1968*a*, *b*]. The difference between cells, which are composed of isolated regions of rising fluid surrounded by a sea of descending material (or vice versa), and rolls, in which regions of ascending and descending fluid are continuously connected, has been pointed out by *Stuart* [1964]. The essence of the theory in Appendix 2 involves the role of the equation of movement of the interface,

$$D\eta/Dt = w(\eta) \tag{8}$$

where the interface is at

$$\eta(x, y, t) \tag{9}$$

and $w(\eta)$ is the vertical velocity at η. When (8) is expanded in a Taylor series about the plane $\eta = h$, we get the equation

$$\frac{\partial\eta}{\partial t} = w(h) + \eta\left.\frac{\partial w}{\partial z}\right|_h - u\left.\frac{\partial\eta}{\partial x}\right|_h - v\left.\frac{\partial\eta}{\partial y}\right|_h + \text{higher orders} \tag{10}$$

When velocity and η are very small, the last four terms are negligible, and yet when the amplitude gets larger, they become relatively larger.

How do solutions to the linear problem in the preceding sec-

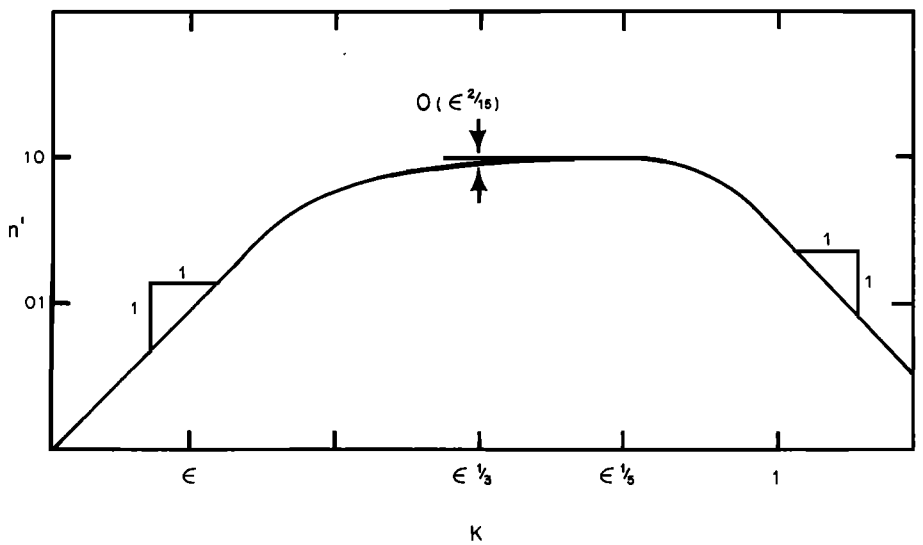

Fig. 4. Normalized growth rate $n' = (4\mu_1 n/g\Delta\rho h)(1 - 0.443\epsilon^{4/5})$ as a function of wave number $K = 4\pi h/\lambda$, where λ is the wavelength for the case where the thin layer is very much more viscous than the deep fluid. Note the broad region between $K = \epsilon^{1/3}$ and $K = \epsilon^{1/5}$ where growth only changes from $1 - \epsilon^{2/3}$ to $1 - 0.443\epsilon^{4/5}$.

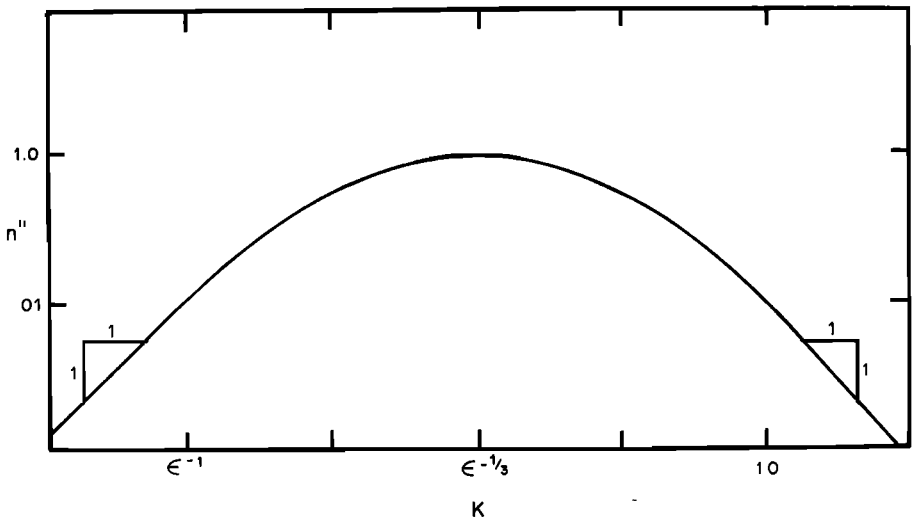

Fig. 5. Normalized growth rate $n'' = \mu_2 n/0.232 g\Delta\rho h$ as a function of wave number $K = 4\pi h/\lambda$, where λ is the wavelength for the case when the thin layer is much less viscous than the deep fluid.

tion affect the quadratic terms? First, we note that if a solution like sin kx or cos kx is inserted into (10), the growth rate is enhanced at a wavelength of $2k$, which is not in the region of maximum linear growth. However, the famous solution

$$\eta = \sum_{n=1}^{3} \cos \mathbf{k}_n \cdot \mathbf{x}$$

where $|k_1| = |k_2| = |k_3 = k_{max}$ and $\mathbf{k}_1 + \mathbf{k}_2 + \mathbf{k}_3 = 0$, enhances the growth rate $\partial\eta/\partial t$ in the vicinity of k_{max} when the three vectors form the sides of an equilateral triangle.

The flow pattern of the above form is sketched in Figure 6 and consists of isolated ascending domes surrounded by a hexagonal matrix of descending material or, alternatively, of isolated descending domes surrounded by a hexagonal matrix of ascending material. Appendix 2 shows how the 'sense' of the hexagons is related to the relative signs of $\partial w/\partial z$ and w from the linear solution in Appendix 1, and how when one layer is very thin, these quantities always have a sign such that fluid protruding from the thin layer has the form of isolated circular domes and fluid intruding into the thin layer has the form of a hexagonal matrix.

The physical reason for the development of such a planform has been mentioned previously by Daneš, although not in connection with the resonant triad that produces the spouts in the hexagonal matrix. The nonlinear terms in (10) sweep fluid toward either the protruding region or the intruding region, depending on the relative signs of w and $\partial w/\partial z$, so as to make one of the two regions larger in cross section than the other. Consequently, the fluid in the constricted region is made to flow more rapidly in order to conserve mass. However, fluid leaving the thin layer can, in fact, flow more rapidly than fluid entering the thin layer, which is slowed by the lower boundary. The fluid leaving the thin layer is concentrated in a circular central region having a much smaller area than the intruding fluid. This solution thus automatically satisfies a constricted flow condition into the thin layer. The reader is urged here to examine Figures 1 and 2 again to verify that the fluid coming out of the layer is indeed very spoutlike in character, like the center of the hexagonal flows in Figure 6.

Formation of Rim Synclines, Overhang, and 'Necking'

After the circular jets have formed as described experimentally in the section on stable layers and physically in the section on the initiation of spouts and after the distortion of the layer approaches that of its depth, the spouts begin a stage of maturation. Experimentally, it was found that the structure henceforth is dependent on the viscosity ratio of the two fluids.

We treat first the case where the upwelling fluid is much more viscous than the fluid being penetrated (Figure 1). Continuity dictates that the velocities be of the same order of magnitude in both fluids, and it can be assumed that the rates of strain of the fluid in both regions are comparable since deformation is caused by movement of the interface. Therefore the stresses due to viscous deformation are proportional to viscosity. When the thin layer is much more viscous, the force balance is between forces due to pressures generated by density differences and forces due to viscous deformation in the upwelling fluid.

The matured jet can therefore be modeled by the viscous fluid being poured from a spout, like syrup being poured from a pitcher. Such a steady viscous jet is shown in Figure 7, in which silicone oil with a viscosity of 60,000 cSt drops through silicone oil with a viscosity of 10 cSt. Notice the similarity between the structures in Figures 1 and 7. The theoretical solution of this flow follows so directly that it does not need to be tested against experiment. We assume little radial dependence, so that the equation of motion is

$$\rho\nu\, \partial^2 w/\partial z^2 = \partial p/\partial z \qquad p = g\Delta\rho z$$

which, when it is integrated, gives $w = (g\Delta\rho/2\rho\nu)z^2 + Az + B$. Far downstream, but not farther than $(g\Delta\rho/\rho\nu^2)^{1/3}$, the radius of the spout can be found from continuity to be

$$r = c/z \tag{11}$$

where c is a constant.

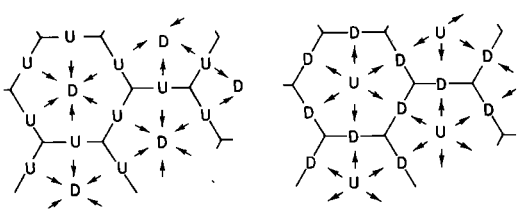

Fig. 6. Sketch of the regions of ascending and descending flows for hexagonal flows, $w = \sum_{n=1}^{3} \cos \mathbf{k}_n \cdot \mathbf{x}$, where $\mathbf{k}$ satisfies the resonant triad. The D denotes downflow; U denotes upflow.

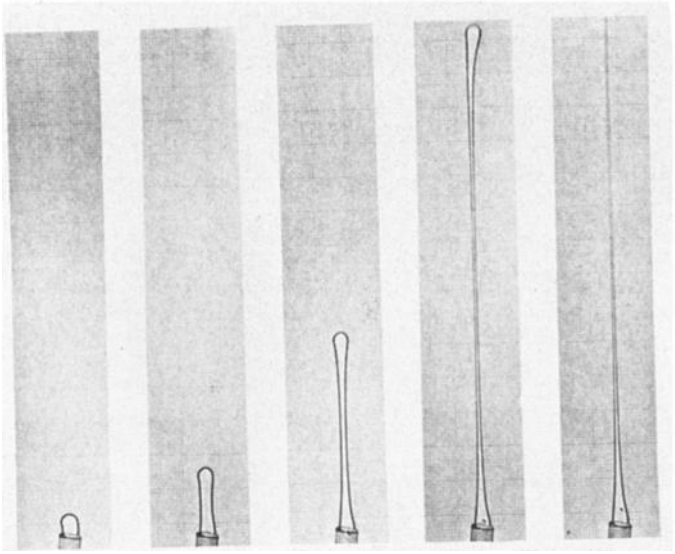

Fig 7. Fluid with a viscosity of 60,000 cSt rising from a spout through fluid with a viscosity of 10 cSt.

In the Rayleigh-Taylor instability the source of fluid is not steady in time but instead is being constantly depleted. It is not hard to modify the theoretical solution (11) to accommodate such a changing source condition, and the jet is still theoretically self-similar. Experimentally, when such a jet is suddenly turned off, the jet begins to gradually decrease its diameter, and yet it retains its identity. A comparison of Figures 1 and 7 shows the similarity between the jet in the Rayleigh-Taylor instability and the jet from a spout.

Before proceeding, we note that the principal effect of surface tension on such a viscous spout is to cause waves to grow and eventually break up the spout into spheres. This breakup was never observed until many minutes had passed in the experiment, when the spouts were about a tenth of their initial radius. It appears that during the three stages of the experiments described here the surface tension has only a small effect on the flows.

We therefore see that there is little tendency for a very viscous dome to develop a plumelike structure with rim synclines that neck off. The nose of the dome can experience a small amount of local widening, which is produced as the dome pushes its way upward through the low-viscosity material, as is shown in Figure 7. In the experiments this dome has been seen to be approximately twice as wide as the viscous pipe that follows it.

When the upwelling fluid is much less viscous than the fluid being penetrated, the structure evolves along a very different sequence. Again, continuity dictates that the rates of strain in both regions are comparable, so that the significant forces are connected with the fluid of greater viscosity. As you might recall from the sequence of photographs in Figure 2, the jet pushes outward into this viscous material, and its nose is subjected to a gradually increasing normal stress that ultimately provides most of the drag equal and opposite to the buoyancy force. By this time, most of the material from the layer has filled a rather large cavity, and a pronounced rim syncline is produced around the cavity. As the pocket of fluid begins to rise, it begins to neck off, since there is no more fluid available to fill the neck. This results in severe necking and a pronounced overhang, which gradually increase until the neck shrinks to a very small size. The bulk of the fluid then rises as almost a perfect sphere, which is a solution to the flow equations of a fluid with small viscosity rising through a fluid of very much larger viscosity, while a small pipe trailing the spherical cavity brings more fluid upward.

This structure looks very much like some of the simpler salt domes. It has been suggested that in the case of salt domes the fluid necks off because the source of fluid is depleted. We believe that this is not the case because the phenomenon of necking is a very basic feature of such flows and does not require a limited source of material. Figure 8 shows 10-cSt oil being fed at a steady rate into a denser silicone oil with a viscosity of 60,000 cSt. Basically, a pocket of fluid forms at the spout and grows until it attains a diameter great enough to buoyantly rise more rapidly than the rate of growth of the radius. The cavity of fluid then rises away, leaving a small pipe that continues to feed the parent cavity.

If the flow is stopped, a neck consisting of small amounts of the lower-viscosity fluid trapped by friction remains long after the initial starting plume has passed. If the flow is reinitiated before this neck completely diffuses away, the old neck offers a path of least resistance, so that the fluid travels up the old neck faster than the initial dome with a nonspherical shape. In Figure 8 two former pipes are visible. In the latter stages of the sequence the circular dome breaks into one of the pipes and rises to the surface quickly.

Experiments were also conducted with two immiscible

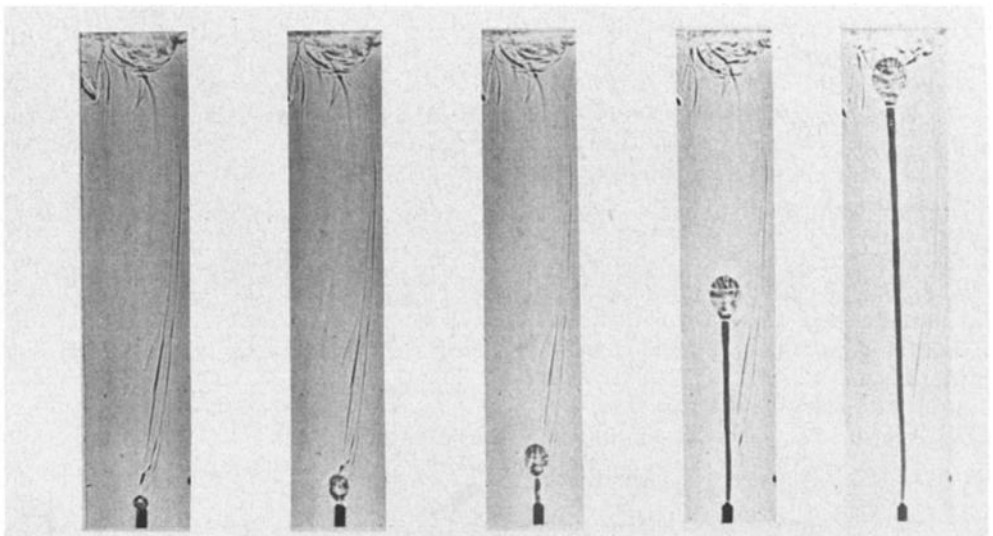

Fig. 8. Fluid with a viscosity of 10 cSt rising from a spout into a fluid with a viscosity of 60,000 cSt.

fluids. For slow flow the trailing pipe did not exist, but instead surface tension closed the pipe off and another sphere began to form. Motor oil with a viscosity of 3.2 cm²/s and a density of 0.86 and silicone oil with a viscosity of 3.7 cm²/s and a density of 0.96 were also used to study the flow that results when viscosities are nearly equal. These two fluids are not miscible but appear to have low interfacial tension. The nose of the resulting spout developed a flow resembling a vortex ring, as is shown in Figure 9. This flow entrained surrounding fluid and is particularly interesting from a fluid dynamic point of view because it exhibited entrainment at a Reynolds number of approximately 2.

A Theory of the Dynamics of Lower-Viscosity Domes and Implications for Salt Domes and Plumes

An approximate theory of the dynamics of the lower-viscosity dome process can be developed by using the Stokes approximation for the rate of ascent (or descent) v of a sphere of radius a, density $\rho \pm \Delta\rho$, and viscosity $\bar{\mu}$ in a fluid of density ρ and viscosity μ [*Batchelor*, 1970].

$$v = \frac{1}{3}\frac{a^2 g}{\mu}(\Delta\rho)\left(\frac{\mu + \bar{\mu}}{\mu + \frac{3}{2}\bar{\mu}}\right) \tag{12}$$

For $\bar{\mu} \ll \mu$, this equation reduces to

$$v = \tfrac{1}{3}(a^2 g \Delta\rho/\bar{\mu}) \tag{13}$$

Suppose that a pipe feeds fluid of viscosity $\bar{\mu}$ into the more viscous fluid at a constant rate Q, as it did in the experiment described at the end of the previous section. If originally the sphere is small enough that $da/dt > v$, it will continue to stay near the source and grow at the rate

$$da/dt = Q/4\pi a^2 \tag{14}$$

The sphere can be expected to rise away from the source after v becomes larger than da/dt, at which time it will have a radius that can be determined by using (13) and (14) as

$$a_0 = (3Q\mu/4\pi g\Delta\rho)^{1/4} \tag{15}$$

The time that it takes to form this sphere is given by $\frac{4}{3}\pi a_0^3/Q$, which is

$$t_0 = (4\pi/3Q)^{1/4}(\mu/g\Delta\rho)^{3/4} \tag{16}$$

After it rises upward, a pipe of fluid will trail the parent cavity. If the introduced fluid is of a much smaller viscosity than the host fluid, the equation of laminar pipe flow is valid in the pipe; this equation is

$$w = \frac{1}{4\bar{\mu}} g\Delta\rho(r_0^2 - r^2)$$

where r_0 is the outside radius of the pipe and r is the distance from the center of the pipe. Mass flux is found by integration to be

$$Q = (\pi/8\bar{\mu})g\Delta\rho r_0^4 \tag{17}$$

and (17) can be inverted to give r_0 as a function of Q:

$$r_0 = (8\bar{\mu}Q/\pi g\Delta\rho)^{1/4} \tag{18}$$

It is observed experimentally that the sphere continues to increase in radius as it rises through the viscous fluid. This increase can be determined by calculating the volume change of the pipe,

$$\pi r_0^2 v = (\pi r_0^2 a^2 g\Delta\rho/3\mu)$$

and by then using continuity to find the increase in volume of the sphere,

$$4\pi a^2 \frac{da}{dt} = \left(Q - \frac{\pi r_0^2 a^2 g\Delta\rho}{3\mu}\right) \tag{19}$$

Before integrating (19), it is convenient to nondimensionalize by using the transformations

$$t_k = (Q/4\pi c^3)^{1/2} t_n$$

$$a_d = (Q/4\pi c)^{1/2} a_n$$

where

$$c = \left(\frac{g\Delta\rho}{16\rho\pi}\frac{Q\bar{\nu}}{\nu^2}\right)^{1/2}$$

subscript d denotes a dimensional variable, and subscript n denotes a nondimensional variable. The nondimensional equations are

$$da/dt = (1/a^2) - 1 \tag{20}$$

where the subscript n has been dropped. No parameters remain in the equation. We note that the growth rate is zero when $a = 1$. This equation can be integrated directly, although the result is algebraically so complicated that it is clearer to integrate it by using finite differences on a hand calculator. Figure 10 shows the final result: it is characterized by $t^{1/3}$ growth in early times ($t \ll (Q/4\pi c^3)^{1/2}$) and maturation to the final size in times of order $(Q/4\pi c^3)^{1/2}$.

In our experiments, with $Q = 0.09$ cm³/s, $g = 980$, $\Delta\rho = 0.042$, $\mu = 600$ cm²/s, and $\bar{\mu} = 0.05$ cm²/s, $c = 9.5 \times 10^{-5}$, the time scale is 90,843 s, and the length scale is 8.6 cm, and so a radius proportional to $t^{1/3}$ should be expected. Figure 10 shows measured radii as a function of time from the data in the experiment shown in Figure 8. An arrow in Figure 10 shows the size of the original diameter of the cavity predicted from (15) as it begins to detach. Examination of the photographs (Figure 8) shows that the process of detachment takes somewhat longer than the idealized model predicts, perhaps owing to drag from the pipe.

In view of the qualitative and quantitative agreement between experiment and theory, it appears safe to conclude that the above theoretical model is reliable for describing the behavior of a viscous fluid rising through a more viscous fluid from a continuous source that is suddenly turned on. We can

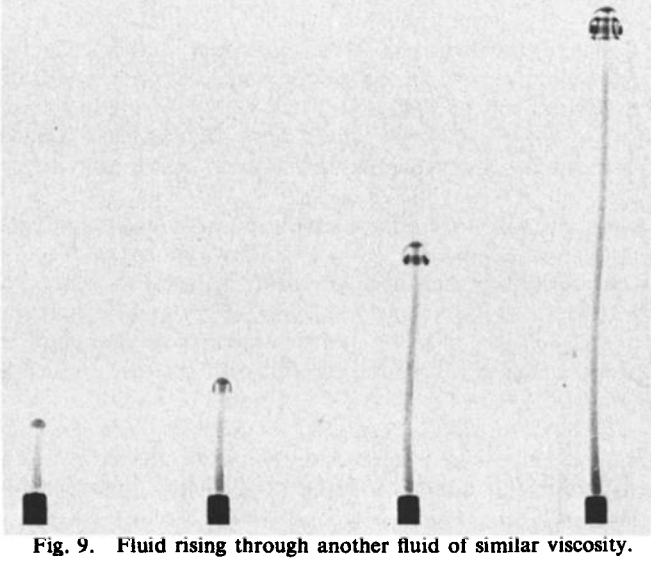

Fig. 9. Fluid rising through another fluid of similar viscosity.

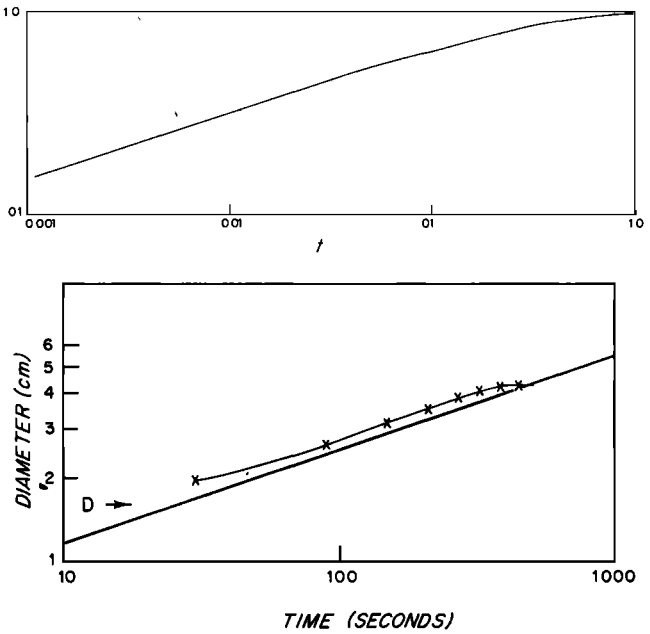

Fig. 10. (Top) Solution to the equation for the growth of a sphere (equation (20)) and (bottom) comparison of the observed radius with the solution to (20) when the dimensionless radius is small.

also add, in passing, that it appears that surface tension plays only a small role in the experiments involving such structures and dynamics on the basis of agreement of data and surface tensionless theory, lack of pinching off of the neck (observed in earlier experiments with glycerin and silicone oil), agreement between the general structures observed in the Rayleigh-Taylor experiments with miscible fluids and the experiments described here with immiscible fluids, and the estimation of the size of the surface tension force to the buoyancy force, given by the so-called Bond number $g\Delta\rho L^2/\sigma$, where σ is surface tension. For the liquids used here, this number is less than one for lengths less than 1 mm, which corresponds only to fine-structure features in this experiment.

Of the thousands of diapiric structures that have been observed throughout the world, many possess features that appear to be typical of the natural flows in the model experiments described here. Others appear to possess nonfluid features, such as extensive tensile fracturing, slippage, and alignment along lines of large faulting. Of those exhibiting fluidlike flow, many could be modeled by a viscous fluid rising through a second fluid of much higher viscosity. Typical features of such an intrusion would be rim synclines, overhang, and necking off. These features have long been known to be characteristic of salt domes. We caution the reader not to compare photographs with seismic cross sections unless the ratio of horizontal distance to vertical distance is 1 : 1.

As was pointed out in the various papers of Selig, Biot, and others, the numbers from linear instability theories of a thin layer with parameters of salt domes ($\epsilon = 10^{-4}$, $\mu_2 = 10^{20}$ P, $\Delta\rho = 0.4$, $h_1 = 300$ m) yield spacings of the order of tens of kilometers and growth times of hundreds of thousands of years, which agree reasonably well with geological observation.

In terms of flows from deep in the mantle, it would be difficult to envisage a sheet of fluid rising through the mantle in view of the fact that the experiments exhibited spouts so early in their history. Since a pocket of low-viscosity fluid was trailed by a pipe, it is also hard to visualize a parade of isolated pockets of low-viscosity fluid rising from a deep source, as has been suggested in association with island arc chains, principally in the Pacific. It may be possible, however, for non-Newtonian or solid processes in the lithosphere to break up such a pipe or to have pockets being formed owing to tilting of the feeder pipe by shear. This stability problem has yet to be studied.

The analysis in this section could be used to determine growth time and size during the starting sequence of deep mantle plumes. The numbers that result from such calculations are dependent on the viscosity and density of the upwelling material, the viscosity of the lower mantle, and the rate of injection of the material at the lower mantle, all relatively unknown properties. One can get some constraints on the permissible values of the properties in which plumes can be expected to have matured. If it is assumed that the parameters are such that the sphere at the top of the plume is still growing when it reaches the surface, the time of ascent through a mantle of thickness h is found by integrating (13) and (14). The resulting formula for time is

$$t = (5\mu h/g\Delta\rho)^{3/5}\,(4\pi/3Q)^{2/5} \tag{21}$$

The numerical values of this formula are plotted in Figure 11 for a plume with a volume flux of 3.3×10^6 cm^3/s in a 3000-km-deep mantle. A plume of this size would overturn the mantle in 1000 b.y. and is roughly twice as big as that producing Hawaii [*Moore*, 1971].

Time is plotted as a function of the poorly known variables, namely, mantle viscosity and plume density. It is evident that the parameter group $\mu/g\Delta\rho$ must be less than 10^{22} for plumes to penetrate the mantle in less than some billions of years. If the viscosity of the mantle is assumed to be 10^{23} P, the density associated with plumes must be at least a percent or two different than that associated with the mantle in order for this inequality to be satisfied.

This analysis is valid if the time given by (21) is less than the time scale used to nondimensionalize (20). In other words, this calculation is valid as long as the sphere at the top of the plume has not reached its maximum radius, which is the length scale used to nondimensionalize (20). In order for this to be true, the ratio of plume viscosity to mantle viscosity must obey the following relationship:

$$(\bar{\nu}/\nu)^{3/4} < 3^{2/5}\,(4/5h)^{3/5}\,(\mu Q/\pi g\Delta\rho)^{3/20} \tag{22}$$

The maximum value of $\bar{\nu}/\nu$ is plotted in Figure 11 on the right axis, and in any circumstance when this ratio is exceeded, the time calculation on the right-hand side of Figure 11 will be too small.

As more aspects of deep mantle convection become clear, it is hoped that the above calculations will be useful. At present, one could conjecture that the processes generating the parameters with the fastest rise times as given here are responsible for the bulk of the plumelike activity observed on the earth.

CONCLUDING REMARKS

We have reviewed here how, when a thin viscous fluid undergoes Rayleigh-Taylor instability into a deep viscous fluid above, the quantitative value of the horizontal wave number is a function of the ratio of the viscosities of the fluids and the growth rates are functions of a number of properties of the fluids. We have also reviewed the well-known theoretical arguments indicating that the flow pattern lacks any

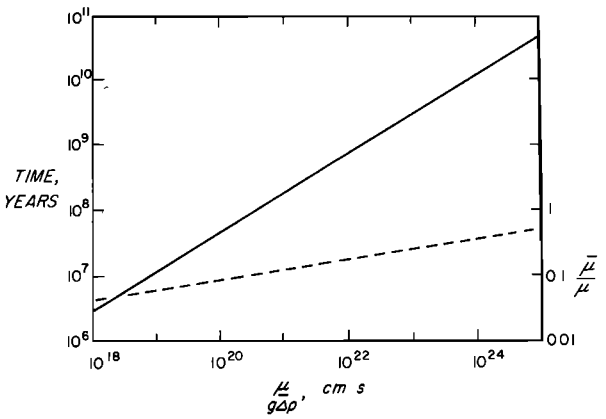

Fig. 11. Time of ascent through the mantle (left abscissa and solid line) as a function of $\mu/g\Delta\rho$, as predicted by the theory for growing low-viscosity domes (equations (13) and (14)). The maximum ratio of plume viscosity to mantle viscosity for which this theory is valid is shown by the right abscissa and the dashed line. If this ratio is exceeded, it will take longer for a plume to rise through the mantle. The mass flux used is 3.3×10^6 cm^3/s.

qualitative structure in the horizontal plane at this level of development.

Second, we have described a theory of how a particular horizontal structure, the hexagonal matrix, develops as the distortion of the previously flat interface becomes significant; this planform is characterized by circular columns of fluid protruding outward from the thin layer irrespective of the viscosity ratio of the two fluids. Such a jetlike structure is a central feature of most natural diapirs.

Third, we have indicated experimentally and argued physically that a viscous diapir rising through a more viscous fluid develops a qualitative structure different from that of a viscous diapir rising through a less viscous fluid. The former is characterized by rim synclines, overhang, and eventual necking off, whereas the latter is characterized by a long horizontal column whose radius decreases with height above the source. Last, we have shown experimentally that a horizontal layer having finite depth generates structures similar to those from a local source that emits material continuously.

We close by noting that it is not clear that all diapiric structures are less viscous than their surrounding media. It would be good to inquire whether granitic batholiths, for instance, rise from their deep origins as a very viscous rheid flow, perhaps being even more viscous than their surroundings, since they are characterized by the absence of overhang and necking.

APPENDIX 1

To provide a foundation for the discussion on nonlinearities in the section on spouts, a linearized analysis of the Rayleigh-Taylor instability will be developed here. The theoretical paths toward such a solution are well trod, and the case of two infinite fluids is developed by *Chandrasekhar* [1961, chap. 10], whose notation we adopt. The specific case of a thin layer underlying a deep layer of finite thickness has been investigated by *Selig* [1965], who emphasized the results that occur when the thin layer is less viscous than the deep layer. Our intent is to provide a convenient foundation for the subsequent discussion of the nonlinear problem. The subscript notation and the coordinates to be used are shown in Figure 3. It will be assumed that the system obeys the incompressible constant-property viscous flow equations, which can be written as

$$\nabla \cdot \mathbf{u} = 0 \tag{A1}$$

$$(\partial/\partial t - \nu\nabla^2)\mathbf{u} = -(1/\rho)\nabla p \tag{A2}$$

where $\mathbf{u}$ is the velocity of the fluid, ν is the kinematic viscosity, and p is the deviation from hydrostatic pressure. These equations can be expected to be valid only for a system in which $U_{max}(L/\nu) \ll 1$, where L is the largest length scale in the problem (in this case the depth of the layer, the wavelength of the perturbation, or $(\nu^2/g)^{1/3}$, where g is gravity). Since fluid velocity in a viscous medium would be proportional to $g\Delta\rho L^2/\rho\nu$, the above criterion could be expected to be valid when $g\Delta\rho L^3/\rho\nu \ll 1$, a criterion easily met in geophysics for all the length scales above. We can immediately write down a class of general solutions to these equations in regions 1 and 2 without considering the details of the movement of the interface. By taking the curl of (A2) and using (A1), the equation for the vertical component of velocity w is

$$(\partial/\partial t - \nu\nabla^2)\nabla^2 w = 0 \tag{A3}$$

Boundary conditions are to be that normal velocity and tangential stress are zero; that is, $w = \partial u/\partial z = 0$ at $z = 0, \hat{z} \to \infty$, which implies that $w = \partial^2 w/\partial z^2 = 0$ at $z = 0, \hat{z} \to \infty$, and which allows solutions in regions 1 and 2 of the following forms:

$$w_1 = (A \sinh kz + B \sinh q_1 z) f(x, y) e^{nt} \tag{A4}$$

$$w_2 = (Ce^{-k\hat{z}} + De^{-q_2\hat{z}}) f(x, y) e^{nt} \tag{A5}$$

where $q_1 = [k^2 + (n/\nu_1)]^{1/2}$, $q_2 = [k^2 + (n/\nu_2)]^{1/2}$, and $\partial^2 f/\partial x^2 + \partial^2 f/\partial y^2 = -k^2 f$. To this order, the analysis admits a multiplicity of solutions, each one's growth rate depending on a two-dimensional wave number vector $\mathbf{k}$ on the x-y plane. This degeneracy will be reduced by the finite amplitude effects in the next section. At the interface, horizontal velocity u, vertical velocity w, tangential stress, and normal stress must be matched. The linearized expressions of these matching conditions are

$$w_1 = w_2 \tag{A6}$$

$$Dw_1 = Dw_2 \tag{A7}$$

$$\mu_1(D^2 + k^2)w_1 = \mu_2(D^2 + k^2)w_2 \tag{A8}$$

$$[\rho_1(\partial/\partial t) - \mu_1(D^2 - k^2)]Dw_1 + 2k^2\mu_1 Dw_1 = [\rho_2(\partial/\partial t) - \mu_2(D^2 - k^2)]\hat{D}w_2 + 2k^2\mu_2\hat{D}w_2 + k^2 g(\rho_2 - \rho_1)\eta \tag{A9}$$

The last condition, (A9), is a balance of normal stress, where the interface is slightly distorted by an amount $\eta(x, y, t) = \hat{z} = z - h$, so that a buoyant force is produced.

The interface is swept along with the fluid so that

$$D\eta/Dt = w(\eta) \tag{A10}$$

For small distortions, (A10) can be expanded in a Taylor series

$$\frac{\partial\eta}{\partial t} + u\frac{\partial\eta}{\partial x} + v\frac{\partial\eta}{\partial y} = w(h) + \eta\frac{\partial w}{\partial z} + \cdots \tag{A11}$$

where w and its derivatives are evaluated at the point $z - h = \hat{z} = 0$. For arbitrarily small η, (A11) reduces to

$$\partial\eta/\partial t = w(h) \tag{A12}$$

Using the solutions given by (A4) and (A5) in (A6)–(A9) and using (A12), we obtain four linear homogeneous equations for the four constants A, B, C, and D.

For a solution to exist, the determinant of the following matrix equation must be equal to zero.

$$\begin{vmatrix} \sinh kh & \sinh q_1h & -1 & -1 \\ k\cosh kh & q_1\cosh q_1h & k & q_2 \\ 2\mu_1k^2\sinh kh & \mu_1(q_1^2+k^2)\sinh q_1h & -2k^2\mu_2 & -\mu_2(k^2+q_2^2) \\ \frac{1}{2}R\sinh kh - C\cosh kh - \alpha_1\cosh kh & \frac{1}{2}R\sinh q_1h - \frac{q_1C}{k}\cosh q_1h & \frac{1}{2}R + C - \alpha_2 & \frac{1}{2}R + \frac{q_2C}{k} \end{vmatrix} \begin{vmatrix} A \\ B \\ C \\ D \end{vmatrix} = 0 \tag{A13}$$

where

$$R = -(gk/n^2)(\alpha_1 - \alpha_2) \qquad C = (k^2/n)(\alpha_1\nu_1 - \alpha_2\nu_2)$$
$$\alpha_1 = \rho_1/(\rho_1+\rho_2) \qquad \alpha_2 = \rho_2/(\rho_1+\rho_2)$$
$$\nu_1 \equiv \mu_1/\rho_1 \qquad \nu_2 = \mu_2/\rho_2$$

Evaluating this determinant will enable us to determine the growth rate n as a function of the horizontal wave number k. The determinant is reduced to a 3×3 by dividing column 1 by $\sinh kh$, dividing column 2 by $\sinh q_1h$, subtracting column 1 from column 2, subtracting column 3 from column 4, and finally adding column 1 to column 3.

It is further reduced to a 2×2 by taking C/k times row 2 and adding it to row 4, dividing columns 2, 3, and 4 by $n\rho_1$, $2(\mu_1 - \mu_2)k^2$, and $n\rho_2$, respectively, multiplying row 4 by $n\rho_1/\alpha_1$, and finally adding column 4 to column 3 and adding column 2 to column 4. Assuming

$$n/\nu_1 \ll k^2 \le 0(1) \qquad n/\nu_2 \ll k^2 \le 0(1)$$

which is equivalent to an assumption of slow viscous flow and is valid when $g\Delta\rho h^3/\rho\nu^2 \ll 1$, where ν is either viscosity. Neglecting terms of order n^2, we can write

$$q_1\coth q_1h - k\coth kh = \tfrac{1}{2}(n/\nu_1k)(\coth kh - kh\,\mathrm{csch}^2 kh) \tag{A14a}$$

$$q_2 - k = n/2\nu_2k \tag{A14b}$$

and the determinant is reduced to the form

$$\begin{vmatrix} \frac{1+\coth kh}{2(\mu_1-\mu_2)k} + \frac{1}{2\mu_2k} & \frac{1}{2\mu_2k} + \frac{1}{2\mu_1k}(\coth kh - kh\,\mathrm{csch}^2 kh) \\ \frac{g\Delta\rho}{2nk(\mu_1-\mu_2)} + \frac{\mu_2+\mu_1}{\mu_2} + 0(n) & \frac{\mu_1}{\mu_2} + \coth kh \end{vmatrix} = 0$$

where $\Delta\rho = \rho_2 - \rho_1$, and it is further reduced to the form

$$n = \frac{g\Delta\rho}{2k\mu_1}\left[\frac{\mu_1 + \mu_2(\coth kh - kh\,\mathrm{csch}^2 kh)}{\mu_1^2(\coth kh + kh\,\mathrm{csch}^2 kh) + \mu_1\mu_2(1+\coth^2 kh) + \mu_2^2(\coth kh - kh\,\mathrm{csch}^2 kh)}\right]$$

We next simplify by putting $\epsilon = \mu_2/\mu_1$ and $2kh = K$ to obtain

$$n = \frac{g\Delta\rho h}{K\mu_1}\left[\frac{\cosh K - 1 + \epsilon(\sinh K - K)}{\sinh K + K + \epsilon(2\cosh K) + \epsilon^2(\sinh K - K)}\right] \tag{A15}$$

The function n clearly has a maximum between the limits $K = 0$ and $K \to \infty$ because for small and large K we find

$$n = g\Delta\rho hK/4\mu_2 \qquad K \ll 1 \qquad K \ll \epsilon$$
$$n = \frac{g\Delta\rho h}{u_1K}\left(\frac{1}{1+\epsilon}\right) + f(\epsilon, e^{-k}) \qquad K \gg 1 \qquad K \gg \epsilon$$

We will now seek the maximum growth rates as a function of the ratio of viscosities, ϵ. For $\epsilon \ll 1$, (A15) has a maximum at

$$K = (180\epsilon)^{1/5} = 2.83\epsilon^{1/5} \tag{A16}$$

Growth rate is

$$n = (g\Delta\rho h/4\mu_1)(1 - 0.443\epsilon^{4/5}) \tag{A17}$$

A sketch of this growth rate is shown in Figure 4, and this growth is characterized by a very broad region of nearly equal growth rate.

For $\epsilon \gg 1$, the wavelength of maximum growth is

$$K = (24/\epsilon)^{1/3} = 2.88\epsilon^{-1/3} \tag{A18}$$

Growth rate is

$$n = (2g\Delta\rho h/3\mu_2)(\epsilon/24)^{1/3} = 0.232(g\Delta\rho h/\mu_2)\epsilon^{1/3} \tag{A19}$$

which has the same power law as a result found earlier by *Selig* [1965]. This growth is sketched in Figure 5.

For $\epsilon = 1$, (A15) reduces to

$$n = \frac{g\Delta\rho}{2\mu_1}\frac{(e^K - 1 - K)}{Ke^K} \tag{A20}$$

which has a maximum at $K = 1.8$ and a growth rate of

$$n = 0.149(g\Delta\rho h/\mu_1) \tag{A21}$$

In summary, we find that the wave number of maximum

growth depends on the ratio of viscosities when this ratio gets either large or small, and the wave number decreases in both of those limits. We also note that in all cases the inequalities before (A14) are satisfied when $g\Delta\rho L^3/\rho\nu^2 \ll 1$, where L is the longest length scale.

APPENDIX 2: THE EFFECT OF NONLINEAR CONVECTION OF THE INTERFACE

Although the wave number and the exponential growth rate were predicted in Appendix 1, more detailed structural features such as the pattern of the domes were beyond the scope of the linearized theory. One effect of noninfinitesimal distortion of the interface occurs in the conditions relating the rate of change of the interface with velocities at the interface. It will be studied here. There are other effects generated by the velocity and stress matching conditions that are beyond the scope of the present study. The expression for the change of the interface is

$$D\eta/Dt = w(\eta) \tag{B1}$$

where w is the vertical velocity of the fluid at the position of the interface $z = \eta(x, y, t)$. We can expand (B1) in a Taylor series at the point $z = h$ and retain terms up to second order as

$$\frac{\partial \eta}{\partial t} = w(h) + \left(\eta \frac{\partial w}{\partial z} - u \frac{\partial \eta}{\partial x} - v \frac{\partial \eta}{\partial y}\right)_h \tag{B2}$$

We will discuss the role of this nonlinearity in conjunction with the solutions in the previous section. The equation set (A6)–(A9) plus solutions of the form

$$w_1 = (A \sinh kz + B \sinh q_1 z) f(x, y, t)$$

$$w_2 = (Ce^{-k\hat{z}} + De^{-q_2\hat{z}}) f(x, y, t)$$

can be reduced to the form

$$[g\Delta\rho h\, \eta(x, y, t)]/K\mu_1 = \{[\sinh k + k + \epsilon(2 \cosh k) + \epsilon^2(\sinh k - k)] \cdot [\cosh k - 1 + \epsilon(\sinh k - k)]^{-1}\} \cdot f(x, y, t) \tag{B3}$$

The right-hand side can be interpreted as the force of friction by the flow field, and the left-hand side can be interpreted as the force of buoyancy. From the evaluation of the previous section, we know that the term in brackets is smallest for the wavelength of fastest growth.

We now ask what solutions can be found for this equation in conjunction with (B2). Substituting for f and using the fact that vorticity in the z direction is zero, we find the relation

$$\frac{\partial \eta}{\partial t} = \frac{g\Delta\rho}{E}\left\{\eta - F\left[\frac{\partial}{\partial x}\left(\eta \frac{\partial \eta}{\partial x}\right) + \frac{\partial}{\partial y}\left(\eta \frac{\partial \eta}{\partial y}\right)\right]\right\} \tag{B4}$$

where E is the term in brackets in (B3) and

$$F = \frac{1}{w}\frac{\partial w}{\partial z}\bigg|_{z=h}$$

We ask what flow configurations would make the right-hand term positive and also would make the above term produce a function with a wave number of minimum E. The function

$$\eta(x, y) = \sum_{n=1}^{3} \cos \mathbf{k}_n \cdot \mathbf{x} \tag{B5}$$

where

$$\mathbf{k}_1 + \mathbf{k}_2 + \mathbf{k}_3 = 0$$

$$|k_1| = |k_2| = |k_3| = k_{\max}$$

can generate a product $\eta(x, y)$ plus some other terms of different wave number. The three wave vectors that satisfy this equation form the sides of an equilateral triangle in k space and represent the familiar hexagonal pattern sketched in Figure 6 if w and $-\partial w/\partial z$ are of opposite sign (on the left) and of the same sign (on the right).

In order to determine the sense of the hexagons, it remains to determine the relative signs of the term w with respect to $\partial w/\partial z$ for the linear solutions in Appendix 1. The linear expression for vertical velocity in the deep fluid, (A5), is

$$w_2 = Ce^{-k\hat{z}} + De^{-q_2\hat{z}} \tag{B6}$$

Hence

$$\partial w_2/\partial z = -kCe^{-k\hat{z}} - q_2 De^{-q_2\hat{z}}$$

We first solve for C as a function of D. Rewriting the first three lines of matrix (A13) as

$$\begin{vmatrix} 1 & 1 & -1 \\ k \coth kh & q_1 \coth q_1 h & k \\ 2\mu_1 k^2 & \mu_1(q_1^2 + k^2) & -2\mu_2 k^2 \end{vmatrix} \begin{vmatrix} A \\ B \\ C \end{vmatrix} = - \begin{vmatrix} -1 \\ q_2 \\ -\mu_2(k^2 + q_2^2) \end{vmatrix} D$$

and solving for C as a function of D give

$$C = \frac{-\begin{vmatrix} 1 & 1 & -1 \\ k \coth kh & q_1 \coth q_1 h & q_2 \\ 2\mu_1 k^2 & \mu_1(q_1^2 + k^2) & -\mu_2(q_2^2 + k^2) \end{vmatrix}}{\begin{vmatrix} 1 & 1 & -1 \\ k \coth kh & q_1 \coth q_1 h & k \\ 2\mu_1 k^2 & \mu_1(q_1^2 + k^2) & -2\mu_2 k^2 \end{vmatrix}} D \tag{B7}$$

We next reduce the determinants to 2 × 2's by adding column 1 to column 3 and subtracting column 1 from column 2. After we use (A14), which are identities for $q_1 \coth q_1h - k \coth kh$ and $q_2 - k$, (B7) reduces to

$$C = -\left(1 + \frac{n}{2k^2\nu_2}\frac{E}{F}\right)D \tag{B8}$$

where

$$E = -\mu_2(\sinh K - K) - \mu_1(\cosh K - 1) \tag{B9}$$

$$F = -\mu_2(\sinh K - K) - \mu_1(\cosh K - 1 + K) \tag{B10}$$

where again $K = 2kh$. For small K, E is $-\mu_1K^2/2$ and F is $-\mu_1K$. Using (B6) and (B8), we find, to order n,

$$\frac{(\partial w_2/\partial z)}{w_2} = \frac{-kc - Dq_2}{C + D} \approx k\left(\frac{E}{F} - 1\right) \tag{B11}$$

and, for small K, we find, using (B9) and (B10), that

$$\frac{(\partial w_2/\partial z)}{w_2} \simeq \frac{1}{2}$$

Therefore $\partial w/\partial z$ and w are in phase, and the fluid protrudes upward into the deep layer as circular jets surrounded by a large region of fluid that sinks in a hexagonal pattern for all viscosity ratios.

We thus see that this nonlinear term speeds the growth of a hexagonal pattern of flow where the central jets come out of the thin layer. Physically, this flow is selected because it adopts a configuration with an unequal cross section between ascending and descending fluids.

We note here that the arguments used in this section apply to a more general problem than that of two viscous fluids, one of finite depth and the other of infinite depth. This particular example was used because of its theoretical tractability.

In the more general case of Rayleigh-Taylor instability, the nonlinear terms expressing convection of the interface do not change, and hence the direction of spouting of the hexagonal flow will still be determined by the relative signs of $\partial w/\partial z$ and w. It is, in fact, possible to calculate a criterion that divides hexagons with one sense from those with the other. We look at the general problem of two fluids of depth h_1 and h_2, density ρ_1 and ρ_2 (not necessarily close together), and viscosity μ_1 and μ_2, where fluid 1 lies below fluid 2. We take our origin at the interface between the fluids, so in order to satisfy free slip conditions at $z = -h_1$ and $z = h_2$, we represent the solution as

$$w_1 = \{A \sinh k(z + h_1) + B \sinh [q_1(z + h_1)]\}g(x, y)e^{nt} \tag{B12}$$

$$w_2 = \{C \sinh k(z - h_2) + D \sinh [q_2(z - h_2)]\}g(x, y)e^{nt} \tag{B13}$$

We note here that it is not necessary to use functions that satisfy free slip conditions at $z = -h_1$ and $z = h_2$, and the analysis outlined here could be used for other boundary conditions. We will set $Dw_1 = Dw_2 = 0$ and ask what trajectory in viscosity-density-depth space allows solutions. This trajectory separates the region where spouts go into fluid 1 from the region where spouts go into fluid 2.

Setting the z derivative of (B12) and (B13) equal to zero and setting $z = 0$ yield the relations

$$A = -\frac{Bq_1 \cosh q_1h_1}{k \cosh kh_1} \tag{B14}$$

$$C = -\frac{Dq_2 \cosh q_2h_2}{k \cosh kh_2} \tag{B15}$$

Substituting these expressions into the expression $w_1 = w_2$ and $\mu_1(D^2 + k^2)w_1 = \mu_2(D^2 + k^2)w_2$ (the equations expressing equality of normal velocities and tangential stress at the interface) yields two relations between B and D, and the condition that these are equivalent reduces to

$$\mu_1 - \frac{n\rho_1 \coth kh_1}{2k(q_1 \coth q_1h_1 - k \coth kh_1)} = \mu_2 - \frac{n\rho_2 \coth kh_2}{2k(q_2 \coth q_2h_2 - k \coth kh_2)} \tag{B16}$$

This is a general criterion valid for all density ratios, viscosities, and depth scales. It is not useful alone until something is known about n as a function of k. Since the buoyancy term has not been used in this derivation, it is generally possible to find a value of gravity that makes any value of n physically possible, given two viscosities, two densities, two depths, and a given k. We will therefore investigate some special cases.

Finite h_1 and h_2 with large viscosities. Equation (B16) reads, when $q \coth qh - k \coth kh = (n/2\nu k)(\coth kh - kh \operatorname{csch}^2 kh)$ is used,

$$\mu_1\left(\frac{K_1}{\sinh K_1 - K_1}\right) = \mu_2\left(\frac{K_2}{\sinh K_2 - K_2}\right) \tag{B17}$$

where $K_1 = 2kh_1$ and $K_2 = 2kh_2$.

We note that if K_2 is infinite and K_1 is finite (the situation studied in detail in this paper), there is no finite nonzero ratio of viscosities that satisfies (B17). This discovery reinforces our calculations in the previous section, which indicated that the fluid always jets out of one of the layers.

The quantitative solution of (B17) depends on the value of K_{max}, but the qualitative structure is easily determined and is shown in Figure B1 as a function of $\epsilon = \mu_2/\mu_1$. Since the solution (B17) is symmetric with respect to an interchange of subscripts 1 and 2, only a half space is shown.

An interesting result is that if we start with $\epsilon > 1$ and K_1 fixed and gradually increase K_2 by increasing the depth of layer 2, there is a reversal of the jets. Since it was shown in the previous section that the jets in layer 1 must jet out of that

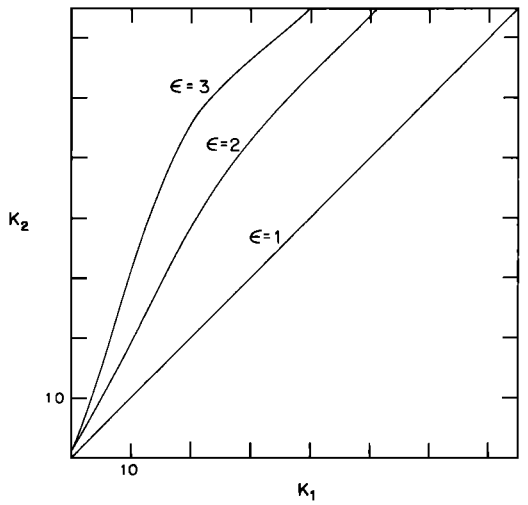

Fig. B1. Trajectories of values of constant ϵ that divide regions of jetting out of region 1 (above the line) from regions of jetting out of region 2 (below the line).

layer as $h_2 \to \infty$, it is thus implied that the jet went into layer 1 when $h_2 = h_1$; i.e., the more viscous fluid would spout into the less viscous fluid when the depths are equal. This hypothesis is borne out by some crude experiments that we did. It is in the opposite sense of the hexagonal flows that exist in a fluid with variable viscosity heated from below, in which the centers of hexagons contain the low-viscosity fluid. The difference is actually due to the fact that the hexagons in this problem have a different physical origin than the hexagons in Rayleigh-Bénard convection. In the former case the hexagons arise from a kinematic effect at the interface, which is simply a lateral convection of the interface toward upwelling or downwelling regions, whereas in the latter case the hexagons arise because they have less friction.

Infinite h_1 and h_2, $\nu_1 = \nu_2$. This case was treated by *Chandrasekhar* [1961], with the results that K_{max} and n_{max} are functions of the density jump. We approximate the coth functions as being very close to 1, set $q_1 = q_2$, and find that (B16) reads

$$\mu_1 - \frac{n\rho_1}{2k(q_1 - k)} = \mu_2 - \frac{n\rho_2}{2k(q_1 - k)} \qquad \text{(B18)}$$

The terms n, k, and q_1 can be determined from Chandrasekhar's Table 46 and are of the form

$$k = \sigma_1(g/\nu^2)^{1/3} \qquad n = \sigma_2(g^2/\nu)^{1/3}$$

$$q_1 = q_2 = k[1 + (\sigma_2/\sigma_1^2)]^{1/2}$$

where σ_1 and σ_2 are order 1 constants that are functions of the density difference between the two layers. When these expressions are substituted, (B18) reads, after some simplification,

$$\mu_1 = \mu_2$$

which is impossible. We therefore would expect jets to exist in this problem going either into or out of the low-density layer, but the exact direction is beyond the scope of this paper.

Acknowledgments. One of us (J.A.W.) would like to thank David Griggs for suggesting this problem and William M. Chappel for advice on the dome problem. The late Paul Cox constructed some of the equipment, and Robert Frazel helped in photographing the structures. During the maturation of this work, one of us (J.A.W.) was supported by the National Science Foundation, Oceanography Section, under grant GA-35447. Contribution 3161, Woods Hole Oceanographic Institution.

REFERENCES

Batchelor, G. K., *An Introduction to Fluid Dynamics*, pp. 236–238, Cambridge University Press, London, 1970.

Berner, H., H. Ramberg, and O. Stephansson, Diapirism in theory and experiment, *Tectonophysics, 15*, 197–218, 1972.

Biot, M. A., Three-dimensional gravity instability derived from two-dimensional solutions, *Geophysics, 31*, 153–166, 1966.

Biot, M. A., and H. Odé, Theory of gravity instability with variable overburden and compaction, *Geophysics, 30*, 213–227, 1965.

Braunstein, J., and G. O'Brien (Eds.), *Diapirism and Diapirs, Mem. 8*, American Association of Petroleum Geologists, Tulsa, Okla., 1968.

Busse, F. H., Das Stabilitätsverhalten der Zellularkonvektion bei endlicher Amplitude, Ph.D. thesis, Ludwig-Maximilian Univ., Munich, Germany, 1962. (English translation by S. H. Davis, *Ref. LT-66-19*, Rand Corp., Santa Monica, Calif., 1966.)

Chandrasekhar, S., *Hydrodynamics and Hydromagnetic Stability*, Oxford University Press, New York, 1961.

Daneš, Z. F., Mathematical formulation of salt dome dynamics, *Geophysics, 29*, 414–424, 1964.

Dobrin, M. B., Some quantitative experiments on a fluid salt dome model and their geological implications, *Eos Trans. AGU, 22*, 528–542, 1941.

Krishnamurti, R. Finite amplitude convection with changing mean temperature, 1, Theory, *J. Fluid Mech., 33*, 445–456, 1968*a*.

Krishnamurti, R., Finite amplitude convection with changing mean temperature, 2, An experimental test of theory, *J. Fluid Mech., 33*, 457–463, 1968*b*.

Moore, J. G., Relationship between subsidence and volcanic load, Hawaii, *Bull. Volcanol., 34*, 562–576, 1971.

Nettleton, L. L., Fluid mechanics of salt domes, *Amer. Ass. Petrol. Geol. Bull., 18*, 1175–1204, 1934.

Parker, T. J., and A. N. McDowell, Model studies of salt-dome tectonics, *Amer. Ass. Petrol. Geol. Bull., 39*, 2384–2470, 1955.

Ramberg, H., Experimental study of gravity tectonics by means of centrifuged models, *Bull. Geol. Inst. Univ. Uppsala, 42*, 1–97, 1963.

Ramberg, H., Model experimentation of the effect of gravity on tectonic processes, *Geophys. J., 14*, 307–329, 1967.

Ramberg, H., Fluid dynamics of layered systems in a field of gravity, a theoretical basis for certain global structures and isostatic adjustment, *Phys. Earth Planet. Interiors, 1*, 63–87, 1968*a*.

Ramberg, H., Instability of layered systems in a field of gravity, 1, 2, *Phys. Earth Planet. Interiors, 1*, 427–474, 1968*b*.

Ramberg, H., Model studies in relation to intrusion of plutonic bodies, *Geol. J. Spec. Issue 2*, 261–286, 1970.

Selig, F., A theoretical prediction of salt dome patterns, *Geophysics, 30*, 633–643, 1965.

Stuart, J. T., On the cellular patterns in thermal convection, *J. Fluid Mech., 18*, 481–498, 1964.

(Received July 8, 1974;
revised October 15, 1974;
accepted October 16, 1974.)